DOI: 10.24352/UB.OVGU-2017-052

TECHNISCHE MECHANIK, 34, 1, (2014), 39 – 50
submitted: September 5, 2013

Microscale Modeling of Magnetoactive Composites Undergoing Large Deformations

C. Spieler, P. Metsch, M. Kästner, V. Ulbricht

This paper is concerned with the development of a material model for the constituents of a magnetoactive composite. Special attention is paid to magnetorheological elastomers which are synthesized from a soft polymeric matrix material with embedded magnetizable particles. Because the particles interact under an applied magnetic load, a coupled magneto-mechanical field problem has to be solved. The mechanical properties of the polymer matrix motivate the consideration of large deformations. We present the balance equations with boundary conditions and an appropriate material model. The corresponding boundary value problems are solved by the Finite-Element-Method. A weak numerical coupling scheme enables the staggered solution of two subproblems, the stationary magnetic and mechanical one. The coupling between both is realized by a surrounding iterative loop.

1 Introduction

Magnetoactive composite materials are in great demand from science, medicine and technology with a special interest on their macroscopic properties. To simulate and predict the effective material properties which are essentially determined by the properties of the individual components and their geometrical arrangement in the composite, a microscopic model accounting for material nonlinearities under the consideration of large deformations is to be provided. The proposed modeling strategy is suitable to capture the behavior of magnetorheological elastomers (MRE) (Davis (1999); Carlson and Jolly (2000)). On the microscale, MRE consist of a cured polymeric matrix with embedded magnetizable particles. During the manufacturing process, before curing the elastomer, the particles are disordered in the absence of an external magnetic load. When a magnetic field is applied, mechanical interactions between the individual particles result in the formation of particle clusters, which are aligned with the direction of the external magnetic field. These microstructural formations influence the effective magnetic and mechanical properties of the composite and motivate their incorporation into the simulation process.
The underlying magneto-mechanical coupling can be classified into three parts. If deformations occur, regardless if they are caused by magnetic or mechanical loads or both, the associated geometry changes influence the magnetic field. On the other hand magnetic terms enter the mechanical subproblem as loads and result in variations of the displacement field. In addition, there is a further coupling effect caused from the material behavior itself. An essential part of modeling MRE is the formulation of proper constitutive relations, both macroscopic and microscopic ones. There are several works focusing on the macroscopic material behavior of MRE obtained by phenomenological observations, see, e.g., Dorfmann and Ogden (2004) or Bustamante (2007). In contrast, the present contribution provides the basis to predict the macroscopic behavior taking into account microscopic aspects by means of a scale transition process. For the computational homogenization a numerical model of a representative volume element accounting for the microstructure has to be generated. In Spieler et al. (2013) we utilize the extended Finite-Element-Method and present a homogenization scheme for magnetoactive composite materials in the context of small deformations. As a preliminary stage for extending this approach to large deformations, this paper focuses on the constitutive modeling and discretization of the local material structure by the Finite-Element-Method (FEM).
Starting with some standard relations of continuum mechanics for large deformations, the balance equations together with jump conditions for the coupled magneto-mechanical boundary value problem (BVP) are formulated in Section 2. Based on thermodynamic considerations a constitutive model is proposed and its parameters are identified by available experimental data. In Section 3 the numerical implementation into a FEM code is explained. The solution of the resulting nonlinear systems of equations requires a linearization. Hence, we specify the expressions needed for the material and geometric tangent stiffness matrices. A comparison with our former small deformation model of two simple problems in Section 4 points out the consequences of the present contribution. The paper is closed by some concluding remarks and an outlook to necessary future work in Section 5.

2 Continuum Formulation of the Problem

In the following section the basic equations of the underlying field problem are presented in a continuum based, phenomenological way. At first the kinematic relations are specified in the context of finite deformations. Based on this, the essential magnetic and coupled mechanical balance equations are formulated with respect to the current configuration together with appropriate jump conditions. In the last part of this section a constitutive model accounting for geometric as well as material nonlinearities for the different constituents of the aforementioned magnetoactive composite material is introduced. Index notation with respect to a Cartesian frame and the EINSTEIN summation convention are applied. Some alternative models describing the microscopic behavior of MRE can be found, e.g., in Galipeau and Ponte Castañeda (2013a,b) as well as Rudykh and Bertoldi (2013).

2.1 Kinematic Relations

A material body $\mathcal{K}$ occupies the domain $\mathcal{B}_0$ with volume V_0 and the boundary $\partial\mathcal{B}_0$ at time $t = t_0$ in its reference configuration. Material points are identified by the coordinates of their position vector $\mathbf{X}$. If loading and deformation occur, the body reaches a current configuration at time t with the domain $\mathcal{B}$, boundary $\partial\mathcal{B}$ and volume V governed by the bijective and continuous mapping $\chi_k = x_k(X_L, t)$. The material particle $\mathbf{X}$ is then located at the spatial position $\mathbf{x}$. The transformation of a differential line element between its reference and current state is described by the deformation gradient

$$F_{kL} = \frac{\partial x_k(X_M, t)}{\partial X_L} = x_{k,L} \quad , \tag{1}$$

where partial derivatives with respect to coordinates are abbreviated by $\frac{\partial(\cdot)}{\partial x_k} = (\cdot)_{,k}$. The determinant of the deformation gradient

$$J = \det(F_{kL}) > 0 \tag{2}$$

is always positive. To get rid of rigid body motions, i.e. rotations still included in $\mathbf{F}$, a polar decomposition is performed yielding the left and right CAUCHY-GREEN deformation tensors

$$b_{kl} = F_{kM}F_{lM} \qquad \text{and} \qquad C_{KL} = F_{mK}F_{mL} \quad . \tag{3}$$

In the limit case of small deformations, the ALMANSI-EULER and GREEN-LAGRANGE strain tensors

$$e_{kl} = \frac{1}{2}\left(\delta_{kl} - b_{kl}^{-1}\right) \qquad \text{and} \qquad E_{KL} = \frac{1}{2}\left(C_{KL} - \delta_{KL}\right) \tag{4}$$

coincide with the infinitesimal strain tensor

$$\varepsilon_{kl} = \frac{1}{2}\left(u_{k,l} + u_{l,k}\right) \quad , \tag{5}$$

which is the symmetric part of the gradient of the displacement vector $\mathbf{u}$.

2.2 Stationary Magnetic Boundary Value Problem

The continuum formulation of the stationary magnetic field problem is given by the MAXWELL equations (Jackson (2006))

$$B_{k,k} = 0 \quad \text{and} \tag{6}$$

$$e_{klm}H_{m,l} = J_k \tag{7}$$

with the magnetic induction $\mathbf{B}$, the magnetic field $\mathbf{H}$ and the vector of free current density $\mathbf{J}$ as well as the third order permutation symbol e_{klm}. The magnetization $\mathbf{M}$ is related to the magnetic induction, the magnetic field and the permeability of free space $\mu_0 = 4\pi e - 7^2$ by

$$B_k = \mu_0(H_k + M_k) \quad . \tag{8}$$

At a surface of discontinuity $\mathcal{S}_\mathrm{d}$, e.g., a material interface, the magnetic field quantities change according to the equations of jump

$$[\![B_k]\!]n_k = 0 \tag{9}$$

$$e_{klm}n_l[\![H_m]\!] = k_k \quad . \tag{10}$$

In the equations above $[\![\phi]\!] = \phi^+ - \phi^-$ is the jump of the physical quantity ϕ across $\mathcal{S}_\mathrm{d}$ with the unit normal vector $\mathbf{n}$ pointing from the subdomain $\mathcal{B}^-$ to $\mathcal{B}^+$. A detailed derivation of the equations of jump is given in the not yet published work Brummund (2013). Equation (9) mathematically represents the continuity of the normal component of the magnetic induction. If no current density $\mathbf{k}$ is present on $\mathcal{S}_\mathrm{d}$, the tangential component of the magnetic field also has to be continuous according to equation (10).
Following Eringen and Maugin (1990), the magnetic field quantities in the reference configuration are given by a set of pull back operations

$$B_K = F_{lK} B_l \tag{11}$$

$$H_K = J F^{-1}_{Kl} H_l \tag{12}$$

$$M_K = J F^{-1}_{Kl} M_l \quad . \tag{13}$$

It should be mentioned that neither the field equations (6) and (7) nor the relation (8) are invariant to the transformations (11)–(13).
One possibility to solve both equations (6) and (7) is the use of the magnetic vector potential $\mathbf{A}$. Its rotation is given by

$$B_k = e_{klm} A_{m,l} \quad . \tag{14}$$

Together with the COULOMB gauge $A_{k,k} = 0$, the vector potential is well-defined. By using the ansatz (14) equation (6) is fulfilled and only equation (7) has to be considered for the solution of the stationary magnetic BVP. Equation (14) and the COULOMB gauge result in the continuity of the vector potential across a surface of discontinuity $[\![A_k]\!] = 0$. The vector potential serves as a primary variable in the FE implementation. On the part $\partial\mathcal{B}_A$ of the external boundary the essential condition

$$A_k = \hat{A}_k \tag{15}$$

is imposed for the k^{th} coordinate of the vector potential. The part of $\partial\mathcal{B}$ with the natural boundary condition (BC)

$$e_{klm} H_m n_l = -\hat{k}_k \tag{16}$$

is labeled $\partial\mathcal{B}_k$. The prescribed value $\hat{\mathbf{k}}$ has to represent the effects of any external magnetic field outside the domain $\mathcal{B}$ and of a surface current $\mathbf{k}$ applied on $\partial\mathcal{B}_k$. For the well-posed definition of the boundary conditions $\partial\mathcal{B}_A \cap \partial\mathcal{B}_k = \varnothing$ and $\partial\mathcal{B}_A \cup \partial\mathcal{B}_k = \partial\mathcal{B}$ have to be valid for each coordinate direction.

2.3 Coupled Mechanical Boundary Value Problem

For the stationary coupled mechanical case the balance of linear momentum

$$t^{\text{tot}}_{kl,k} + \varrho f_l = 0 \tag{17}$$

and angular momentum

$$e_{klm} t^{\text{tot}}_{lm} = 0 \tag{18}$$

equilibrate the total stress tensor $\mathbf{t}^{\text{tot}}$. In equation (17) $\varrho\mathbf{f}$ is the mechanical body force density with the mass density of the current configuration ϱ. According to equation (18) the total stress tensor is symmetric. It can be split additively in the sum of the mechanical stress tensor $\mathbf{t}$ and a magnetic contribution $\mathbf{t}^{\text{m}}$, i.e. $t^{\text{tot}}_{kl} = t_{kl} + t^{\text{m}}_{kl}$. This decomposition is not free of arbitrariness. We use the magnetic stress tensor

$$t^{\text{m}}_{kl} = \frac{1}{\mu_0} B_k B_l - \frac{1}{2\mu_0} B_m B_m \delta_{kl} - B_k M_l + B_m M_m \delta_{kl} \quad , \tag{19}$$

which is microscopically motivated by de Groot and Suttorp (1972). In the absence of any magnetization, i.e. vacuum with $M_k = 0$, $\mathbf{t}^{\text{m}}$ reduces to the MAXWELL stress tensor. Furthermore, the used decomposition is compatible with phenomenological requirements. In general, i.e. for anisotropic magnetic material behavior, equation (18) results in an unsymmetric mechanical stress tensor $e_{klm}(t_{lm} - B_l M_m) = 0$.
Based on the continuity of the displacement field and the jump equation of the total traction vector

$$[\![u_k]\!] = 0 \tag{20}$$

$$[\![t^{\text{tot}}_{kl}]\!] n_k + p_l = 0 \quad , \tag{21}$$

the following boundary conditions are specified. On $\partial\mathcal{B}_u$ the essential condition

$$u_k = \hat{u}_k \tag{22}$$

is formulated for the k^{th} coordinate of the displacement vector. The natural boundary condition

$$t_{kl}^{\text{tot}} n_k = \hat{p}_l \tag{23}$$

is prescribed on $\partial\mathcal{B}_p$, where the effective surface load $\hat{\mathbf{p}}$ has to account for any contribution from mechanical and magnetic tractions outside $\mathcal{B}$ as well as an applied mechanical surface load $\mathbf{p}$. In addition $\partial\mathcal{B}_u \cap \partial\mathcal{B}_p = \varnothing$ and $\partial\mathcal{B}_u \cup \partial\mathcal{B}_p = \partial\mathcal{B}$ hold for each coordinate.
Introducing the mass density with respect to the reference configuration ϱ_0, the local form of the balance of mass results in the relation

$$J = \frac{\varrho_0}{\varrho} \quad . \tag{24}$$

A thermodynamically consistent constitutive model, presented in the following subsection, is derived on the basis of the CLAUSIUS-DUHEM inequality

$$-\varrho\left(\dot{\psi} + \dot{T}s\right) + t_{kl}F_{Mk}^{-1}\dot{F}_{lM} - M_k\dot{B}_k - \frac{q_k}{T}T_{,k} + J_kE_k \geq 0 \quad , \tag{25}$$

where ψ is the specific free energy, T the absolute temperature, s the specific entropy, $\mathbf{q}$ the heat flux vector and $\mathbf{E}$ the electric field. The material time derivative is abbreviated by $\dot{(\cdot)}$. A detailed discussion leading to equation (25) is presented, e.g., in Eringen and Maugin (1990) as well as Dorfmann and Ogden (2003).

2.4 Constitutive model

To conform with the principle of material objectivity, we choose the specific free energy to depend on the right CAUCHY-GREEN deformation tensor $\mathbf{C}$, the reference magnetic induction $\mathbf{B}_0$ and the absolute temperature T. There is no internal structure to be considered for the microscopic material point which confirms with the assumption of isotropic material behavior. In this situation the dependency on $\mathbf{C}$ can be expressed in terms of its three principal invariants I_α^C with $\alpha \in \{1,2,3\}$ and $I_1^C = C_{KK}$, $I_2^C = \frac{1}{2}\left(C_{KK}C_{LL} - C_{KL}C_{KL}\right)$ and $I_3^C = \det\left(C_{KL}\right) = J^2$. Assuming that the material behavior is independent of the electric field and the temperature gradient, the CLAUSIUS-DUHEM inequality is reformulated to

$$-\varrho\left[\frac{\partial\psi}{\partial F_{lM}}\dot{F}_{lM} + \frac{\partial\psi}{\partial B_K}\dot{B}_K + \frac{\partial\psi}{\partial T}\dot{T} + \dot{T}s\right] + \left(t_{kl} + M_kB_l\right)F_{Mk}^{-1}\dot{F}_{lM} - \frac{1}{J}M_K\dot{B}_K \geq 0 \tag{26}$$

and

$$-\frac{q_k}{T}T_{,k} + J_kE_k \geq 0 \quad . \tag{27}$$

According to the procedure of Coleman and Noll (1963) the constitutive relations

$$_{\text{E}}t_{kl} = \varrho F_{kM}\frac{\partial\psi(I_\alpha^C, B_Q, T)}{\partial F_{lM}} = t_{kl} + M_kB_l \quad , \tag{28}$$

$$M_K = -\varrho_0\frac{\partial\psi(I_\alpha^C, B_Q, T)}{\partial B_K} \quad \text{and} \tag{29}$$

$$s = -\frac{\partial\psi(I_\alpha^C, B_Q, T)}{\partial T} \tag{30}$$

are derived from the inequality (26) and define the material behavior in a proper way, if the potential ψ exists. Henceforth only isothermal processes are to be considered and the relations (27) and (30) are out of discussion. Bustamante et al. (2008) point out constitutive equations differing from the one presented above and mention the diversity of equivalent formulations in literature. Equation (28) motivates an alternative split of the total stress tensor into two symmetric parts

$$t_{kl}^{\text{tot}} = {}_{\text{E}}t_{kl} + \hat{t}_{kl} \quad . \tag{31}$$

The stress tensor $\hat{\mathbf{t}}$ is related to the magnetic stress by

$$\hat{t}_{kl} = t_{kl}^{\text{m}} - M_kB_l \quad . \tag{32}$$

In the present work we assume an additive decomposition of the specific free energy which can be expressed by

$$\psi(I_\alpha^C, B_Q) = \psi^{\text{mag}}(B_Q) + \psi^{\text{mech}}(I_\alpha^C) \quad . \tag{33}$$

In equation (33) ψ^{mag} is independent of any deformation and ψ^{mech} is not influenced by a magnetic field. The embedded magnetizable particles are very stiff compared to their surrounding matrix. The expected strains in the

particles due to loading of the magnetoactive composite will be very small. On the other hand the elastomer material is supposed to be nonmagnetizable. These assumptions approximately agree with the analytical description of rigid magnetizable inclusions in a nonmagnetizable elastomer, see Ponte Castañeda and Galipeau (2011).

Magnetic part of the potential

The material modeling is motivated by experimental data covering the magnetization behavior of the carbonyl iron powder BASF CIP CC illustrated in Figure 1. These particles are used in the mentioned MRE. The analyzed material exhibits a nonlinear magnetization curve with negligible hysteresis effects. It is assumed that the measurement represents the behavior of the referential values $\mathbf{M}_0$ and $\mathbf{B}_0$. During the experimental characterization with a vibration sample magnetometer no relevant deformation of the magnetic specimen is generated and measured. An appropriate nonlinear phenomenological model is then given by the isotropic relation

$$M_K = M_\mathrm{s} \tanh\left(\delta B_0\right) \frac{B_K}{B_0} \quad , \tag{34}$$

where M_s is the saturation magnetization, δ a scaling parameter and $B_0 = \sqrt{B_K B_K}$ the absolute value of the reference magnetic induction. A linearization of equation (34) in the neighborhood of $B_0 = 0$, yields the linear relation

$$M_K = \chi_B B_K \tag{35}$$

with the susceptibility $\chi_B = M_\mathrm{s}\delta$. Both, the nonlinear and the linearized model are plotted in Figure 1. The linear model is able to represent the experimental data within a range of $B_0 \lesssim 0.5$. After that, the saturation becomes dominant which is captured by the proposed nonlinear model (34). Integrating the expressions (34) and (35) according to the constitutive relation (29) results in the potential

$$\psi^\mathrm{mag} = -\frac{M_\mathrm{s}}{\varrho_0 \delta} \ln\left[\cosh\left(\delta B_0\right)\right] \tag{36}$$

for the magnetic nonlinear case and

$$\psi^\mathrm{mag} = -\frac{1}{2\varrho_0} \chi_B B_0^2 \tag{37}$$

for linear magnetic material behavior. Because ϱ_0 and B_0 are fixed referential values, the derivative of ψ^mag with respect to the deformation gradient $\mathbf{F}$ according to equation (28) is, as implied, not connected to any stress contribution.

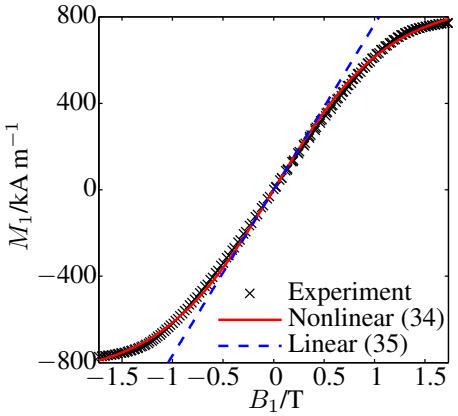

Figure 1. Magnetization behavior of BASF CIP CC

Mechanical part of the potential

In order to capture finite deformations, which can occur in the magnetoactive composite, a hyperelastic material model is proposed. By inserting ψ according to equation (33) in equation (28), the relation

$${}_\mathrm{E}t_{kl} = 2\varrho \left[\frac{\partial \psi^\mathrm{mech}}{\partial I_1^C} b_{kl} + \frac{\partial \psi^\mathrm{mech}}{\partial I_2^C} \left(I_1^C b_{kl} - b_{km} b_{ml} \right) + \frac{\partial \psi^\mathrm{mech}}{\partial I_3^C} I_3^C \delta_{kl} \right] \tag{38}$$

is obtained. A very general and commonly used function ψ^mech describes the OGDEN material (Ogden (1997)). In the present work a compressible form of the neo-HOOKEan material, which is a special case of the OGDEN

material, with the potential

$$\psi^{\text{mech}} = \frac{1}{2\varrho_0}\left[\mu\left(I_1^C - \ln I_3^C - 3\right) + \frac{\lambda}{2}\left(I_3^C - \ln I_3^C - 1\right)\right] \tag{39}$$

and the LAMÉ parameters μ and λ is used. The symmetric stress ${}_{\text{E}}\mathbf{t}$ is then given by

$${}_{\text{E}}t_{kl} = \frac{1}{J}\left[\mu\left(b_{kl} - \delta_{kl}\right) + \frac{\lambda}{2}\left(I_3^C - 1\right)\delta_{kl}\right] \quad , \tag{40}$$

which reduces to the classical HOOKEan law

$${}_{\text{E}}t_{kl} = 2\mu\varepsilon_{kl} + \lambda\varepsilon_{mm}\delta_{kl} \tag{41}$$

in the case of small deformations, see also Eringen and Maugin (1990). It has to be remarked that only for nonmagnetizable materials the stress tensor ${}_{\text{E}}\mathbf{t}$ according to equation (40) or (41) equals the mechanical stress tensor $\mathbf{t}$.

3 Finite Element Formulation of the Problem

The numerical solution of the underlying systems of partial differential equations is accomplished by the FEM. In this section first the implemented numerical coupling scheme is explained, followed by the weak forms of the corresponding BVP. A linearization of the resulting nonlinear systems of equations enables an iterative solution procedure with the NEWTON-RAPHSON method. Vectors and matrices in the FE formulation are labeled by single and double underlined bold symbols $\underline{\mathbf{a}}$ and $\underline{\underline{\mathbf{a}}}$, respectively.

For simplicity and demonstration purposes, only problems homogeneous in the third direction will be considered. In this two-dimensional case $A_1 = A_2 = 0$ is an appropriate choice and the vector potential $\mathbf{A}$ contains only one nonzero component A_3. Since there are no gradients in the third direction, the COULOMB gauge is fulfilled and has not to be considered furthermore.

3.1 Numerical Coupling Scheme

There are different approaches to treat the coupled field problem numerically. In the present work a weak numerical coupling, also known as load vector, sequential, partitioned or staggered coupling, is adopted. The underlying algorithm is schematically presented in Figure 2. An incremental analysis starts by prescribing the boundary conditions and solving the magnetic BVP with respect to the undeformed reference configuration. With this known solution the mechanical BVP is analyzed. After each pass of both calculations a convergence criterion is checked, i.e. the corrections of the primary field variables vector potential $\Delta\underline{\mathbf{A}}$ and displacement $\Delta\underline{\mathbf{u}}$ are compared to their incremental changes. If these relative changes are smaller than a termination value, the solution is said to be in equilibrium and the analysis continues with the next increment by updating the BC. Otherwise the configuration is updated and both field problems are solved again. To reach a converged state, at least two cycles have to be passed. In the mechanical subsystem magnetic variables are assumed to be fixed and vice versa in the magnetic subproblem the deformation does not change. The benefits of this coupling scheme are the ease of implementation and the smaller symmetric system matrices compared to a monolithic or strongly coupled approach. In our previous works (Kästner et al. (2013) and Spieler et al. (2013)), which are limited to small deformations, no update of the configuration is performed and the check for convergence is dispensable.

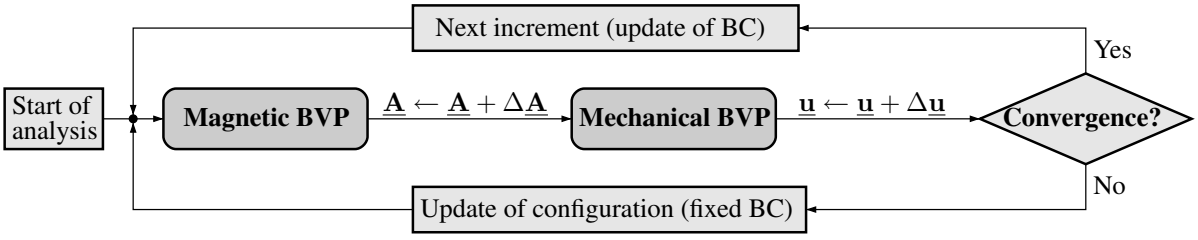

Figure 2. Implemented numerical coupling scheme with staggered solution strategy

3.2 Linearization of the Weak Forms and Discretization

Starting with equation (7) multiplied by a weight function, i.e. the virtual potential δA_k which fulfills $\delta A_k = 0$ on $\partial\mathcal{B}_A$, integration by parts and using the relations (14) and (16), the weak form of the magnetic subsystem

$$\int_{\mathcal{B}} H_k \delta B_k \,\mathrm{d}V - \int_{\mathcal{B}} j_k \delta A_k \,\mathrm{d}V - \int_{\partial\mathcal{B}_k} \hat{k}_k \delta A_k \,\mathrm{d}S = 0 \tag{42}$$

is derived. For an iterative solution of the underlying FE system, a linearization of equation (42) is required. It is assumed that the external loads, expressed by the last two terms in the equation above, are independent of changes in $\mathbf{A}$ but in general the magnetic field strength $\mathbf{H}$ depends nonlinearly on the vector potential. By applying the chain rule of differentiation the expression

$$\frac{\partial H_k}{\partial B_l} = \begin{cases} \dfrac{1}{\mu_0}\delta_{kl} - \dfrac{1}{J}\chi_B b_{kl} & \text{for linear material (35)} \\ \dfrac{1}{\mu_0}\delta_{kl} - \dfrac{M_\mathrm{s}}{JB_0}\tanh(\delta B_0) b_{kl} & \\ \quad + \dfrac{M_\mathrm{s}}{JB_0^2}\left[\dfrac{\tanh(\delta B_0)}{B_0} - \dfrac{\delta}{\cosh^2(\delta B_0)}\right] b_{km} b_{lq} B_m B_q & \text{for nonlinear material (34)} \end{cases} \tag{43}$$

defines the magnetic material tangent $\mathbf{C}^{\mathrm{mag}}$.
Using a standard isoparametric FE approximation with the matrix of shape functions $\underline{\underline{\mathbf{N}}}^{\mathrm{mag}}$ and their partial derivatives according to equation (14) expressed by $\underline{\underline{\mathbf{B}}}^{\mathrm{mag}}$, the weak form (42) of n_e assembled elements is now given by the discrete RITZ formulation

$$\delta\underline{\mathbf{A}}^{\mathrm{T}} \Bigg[\underbrace{\bigcup_{i=1}^{n_\mathrm{e}} \left(\int_{\mathcal{B}_i^\mathrm{e}} \underline{\underline{\mathbf{B}}}^{\mathrm{mag}^{\mathrm{T}}} \underline{\mathbf{H}} \,\mathrm{d}V \right)}_{\underline{\mathbf{j}}^{\mathrm{int}}} \underbrace{- \bigcup_{i=1}^{n_\mathrm{e}} \left(\int_{\mathcal{B}_i^\mathrm{e}} \underline{\underline{\mathbf{N}}}^{\mathrm{mag}^{\mathrm{T}}} \underline{\mathbf{j}} \,\mathrm{d}V \right) - \bigcup_{i=1}^{n_\mathrm{e}} \left(\int_{\partial\mathcal{B}_i^\mathrm{e}} \underline{\underline{\mathbf{N}}}^{\mathrm{mag}^{\mathrm{T}}} \hat{\underline{\mathbf{k}}} \,\mathrm{d}S \right) - \underline{\mathbf{j}}^*}_{-\underline{\mathbf{j}}^{\mathrm{ext}}} \Bigg] = \underline{\mathbf{0}} \quad . \tag{44}$$

In the equation above the vector $\underline{\mathbf{j}}^*$ accounts for discrete nodal loads typically applied in FE analysis. From the argument of arbitrary but admissible virtual potentials $\delta\underline{\mathbf{A}}$, finally the nonlinear FE system is defined by the vanishing difference of the internal and external loads $\underline{\mathbf{j}}^{\mathrm{int}} - \underline{\mathbf{j}}^{\mathrm{ext}} = \underline{\mathbf{0}}$. Its incremental and iterative solution with the NEWTON-RAPHSON method is based on the linearized relation

$$\underline{\underline{\mathbf{K}}}^{\mathrm{mag}} \Delta\underline{\mathbf{A}} = \underline{\mathbf{j}}^{\mathrm{ext}} - \underline{\mathbf{j}}^{\mathrm{int}} \quad , \tag{45}$$

where the magnetic tangent stiffness matrix

$$\underline{\underline{\mathbf{K}}}^{\mathrm{mag}} = \bigcup_{i=1}^{n_\mathrm{e}} \left(\int_{\mathcal{B}_i^\mathrm{e}} \underline{\underline{\mathbf{B}}}^{\mathrm{mag}^{\mathrm{T}}} \underline{\underline{\mathbf{C}}}^{\mathrm{mag}} \underline{\underline{\mathbf{B}}}^{\mathrm{mag}} \mathrm{d}V \right) \tag{46}$$

contains the deformation dependent material tangent (43).
The weak form of the coupled mechanical subsystem

$$\int_{\mathcal{B}} {}_\mathrm{E} t_{kl} \delta u_{l,k} \,\mathrm{d}V - \int_{\mathcal{B}} \left(\varrho f_k \delta u_k - \hat{t}_{kl} \delta u_{l,k} \right) \mathrm{d}V - \int_{\partial\mathcal{B}_p} \hat{p}_k \delta u_k \,\mathrm{d}S = 0 \tag{47}$$

is obtained from equations (17) and (23) with the split of the total stress tensor according to equation (31). In the equation above δu_k is the virtual displacement satisfying $\delta u_k = 0$ on $\partial\mathcal{B}_u$. Again we assume that the external forces, expressed through the last two integrals in equation (47), are independent of changes in the primary field variable $\underline{\mathbf{u}}$. The approximation and FE discretization with the matrices of shape functions $\underline{\underline{\mathbf{N}}}^{\mathrm{mech}}$ and their partial derivatives included in $\underline{\underline{\mathbf{B}}}^{\mathrm{mat}}$ (according to the kinematic relations) and the afterwards used matrix $\underline{\underline{\mathbf{B}}}^{\mathrm{geo}}$ (contains

the partial derivatives of $\underline{\underline{\mathbf{N}}}^{\text{mech}}$ with respect to the spatial coordinates) yields

$$\delta\underline{\mathbf{u}}^{\mathrm{T}}\left[\underbrace{\bigcup_{i=1}^{n_{\mathrm{e}}}\left(\int_{\mathcal{B}_i^{\mathrm{e}}}\underline{\underline{\mathbf{B}}}^{\text{mat}^{\mathrm{T}}}\,{}_{\mathrm{E}}\underline{\mathbf{t}}\,\mathrm{d}V\right)}_{\underline{\mathbf{f}}^{\text{int}}}\underbrace{-\bigcup_{i=1}^{n_{\mathrm{e}}}\left(\int_{\mathcal{B}_i^{\mathrm{e}}}\left(\underline{\underline{\mathbf{N}}}^{\text{mech}^{\mathrm{T}}}\varrho\underline{\mathbf{f}}-\underline{\underline{\mathbf{B}}}^{\text{mat}^{\mathrm{T}}}\hat{\underline{\mathbf{t}}}\right)\mathrm{d}V\right)-\bigcup_{i=1}^{n_{\mathrm{e}}}\left(\int_{\partial\mathcal{B}_i^{\mathrm{e}}}\underline{\underline{\mathbf{N}}}^{\text{mech}^{\mathrm{T}}}\hat{\underline{\mathbf{p}}}\,\mathrm{d}S\right)-\underline{\mathbf{f}}^{*}}_{-\underline{\mathbf{f}}^{\text{ext}}}\right]=\underline{\mathbf{0}} \tag{48}$$

for the weak form (47) of the coupled mechanical subsystem. Because the proposed constitutive model (40) for the stress tensor ${}_{\mathrm{E}}\mathbf{t}$ is equivalent to the ordinary neo-HOOKEan material for large deformation processes, the standard procedure of linearization within the FEM is applied, see among others Zienkiewicz and Taylor (2005) or Belytschko et al. (2000). The linearization of the first term in equation (47) is performed according to the concept of directional derivatives proposed by Hughes and Pister (1978). It is therefore reasonable to express the integral and the stress tensor ${}_{\mathrm{E}}\mathbf{t}$ with respect to the reference configuration. Performing the linearization under consideration of the product rule of differentiation results in two contributions to the tangent, a geometrical and material part. Further details are to be found in the aforementioned literature. Finally the iterative solution of the nonlinear system of equations $\underline{\mathbf{f}}^{\text{int}}-\underline{\mathbf{f}}^{\text{ext}}=\underline{\mathbf{0}}$ is based on the linearized expression

$$\left[\underline{\underline{\mathbf{K}}}^{\text{mat}}+\underline{\underline{\mathbf{K}}}^{\text{geo}}\right]\Delta\underline{\mathbf{u}}=\underline{\mathbf{f}}^{\text{ext}}-\underline{\mathbf{f}}^{\text{int}} \tag{49}$$

with the material part of the tangent stiffness matrix

$$\underline{\underline{\mathbf{K}}}^{\text{mat}}=\bigcup_{i=1}^{n_{\mathrm{e}}}\left(\int_{\mathcal{B}_i^{\mathrm{e}}}\underline{\underline{\mathbf{B}}}^{\text{mat}^{\mathrm{T}}}\underline{\underline{\mathbf{C}}}^{\text{mech}}\underline{\underline{\mathbf{B}}}^{\text{mat}}\,\mathrm{d}V\right)\quad, \tag{50}$$

where the material tangent is defined by

$$\underline{\underline{\mathbf{C}}}^{\text{mech}}=\frac{1}{J}\begin{bmatrix}2\mu+\lambda & \lambda J^2 & 0\\ \lambda J^2 & 2\mu+\lambda & 0\\ 0 & 0 & \mu-\dfrac{\lambda}{2}\left(J^2-1\right)\end{bmatrix} \tag{51}$$

for the assumption of plane strain. The corresponding three-dimensional material tangent can be found in Wriggers (2008). Submatrices of the geometrical tangent stiffness matrix $\underline{\underline{\mathbf{K}}}^{\text{geo}}$ are computed from the relation

$$\underline{\underline{\mathbf{K}}}_{ab}^{\text{geo}}=\bigcup_{i=1}^{n_{\mathrm{e}}}\underline{\mathbf{I}}H_{ab}\quad, \tag{52}$$

with the two by two identity matrix $\underline{\mathbf{I}}$ and the matrix

$$\underline{\underline{\mathbf{H}}}=\int_{\mathcal{B}_i^{\mathrm{e}}}\underline{\underline{\mathbf{B}}}^{\text{geo}^{\mathrm{T}}}\,{}_{\mathrm{E}}\underline{\mathbf{t}}\,\underline{\underline{\mathbf{B}}}^{\text{geo}}\,\mathrm{d}V\quad. \tag{53}$$

The described element formulation is implemented for two-dimensional quadrilateral elements with bilinear and biquadratic shape functions.

4 Numerical Examples

In the following section the proposed modeling strategy is applied to two heterogeneous microstructural arrangements which are schematically depicted in Figures 3 and 4. Both BVP are defined and their numerical solutions are obtained with the FE formulation presented in the preceding Section 3 under the assumptions of plane strain. A comparison of selected results with the ones of a small deformation model (Kästner et al. (2013); Spieler et al. (2013)) for magnetic linear and nonlinear material behavior points out the need and advantage of the present contribution.

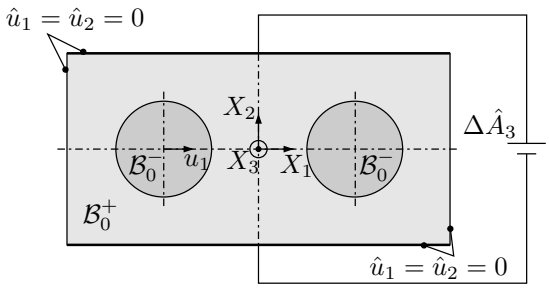

Figure 3. Two interacting circular inclusions with linear vector potential BC

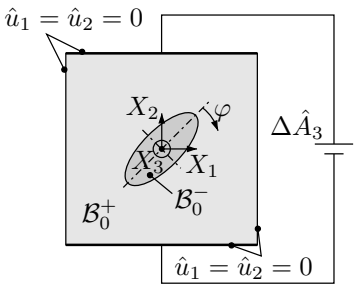

Figure 4. Reorientation of an elliptic inclusion with linear vector potential BC

4.1 Two Interacting Circular Inclusions

Motivated by chain-like particle structures occurring in oriented magnetorheological elastomers, the interaction between two circular inclusions is investigated under the consideration of large deformations. The domain of interest, which is illustrated in Figure 3, has a size of 20×10. Both embedded circular inclusions have a radius of 2.49 and an initial distance of 10. They are characterized by the parameters $E^- = 210$, $\nu^- = 0.3$, $M_s^- = 868$ and $\delta^- = 0.883$ or $\chi_B^- = 767$ for the magnetic nonlinear or linear case, respectively. $E^+ = 75$, $\nu^+ = 0.4$ and $\chi_B^+ = 0$ are assigned to the soft matrix material.
On the whole boundary the displacement is fixed and a linear vector potential with a difference of $\Delta\hat{A}_3 = 14$ (bounded by the range of experimental magnetization data for the nonlinear material model, see Figure 1) between the upper and lower boundary is prescribed within 20 equidistant increments, resulting in an effective magnetic field pointing into the X_1-direction. The inclusions become magnetized inhomogeneously. As a consequence a resultant force, acting on each particle, causes their attraction. Figure 5 (a) shows the computed displacement u_1 of the point with the material coordinates $X_1 = -5$ and $X_2 = 0$ depending on the external load $\Delta\hat{A}_3$. There is a significant difference between the curves distinguished by the magnetic linear and nonlinear behavior. This material nonlinearity, caused by magnetic saturation effects, bounds the attractive forces and consequently the displacement of the inclusions. In both cases the large deformation model yields larger deformations because the smaller the distance between the particles will be, the larger the net attractive forces become. This change of configuration is not incorporated in the small deformation model. An impact of the different models on the magnetic field variables is expressed by the magnetic induction B_1 of the point $X_1 = X_2 = 0$ in Figure 5 (b). Again the influence of the saturation is obvious. If the particles get closer, the field lines between them are more concentrated which is an effect of the present configuration dependency.

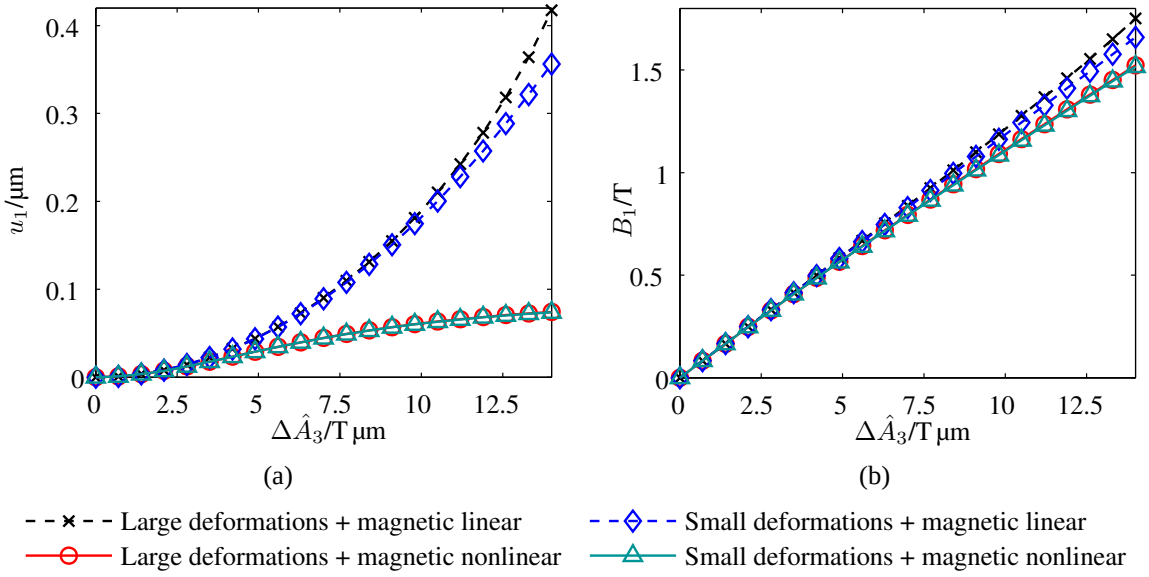

Figure 5. Numerical results of attracting inclusions: (a) horizontal displacement of the left particle's center and (b) magnetic induction B_1 at the point $X_1 = X_2 = 0$

4.2 Reorientation of an Elliptic Inclusion

Beside the geometric arrangement, another important aspect of real microstructural particle compounds is the shape of each individual inclusion, e.g., if it differs from an often assumed idealized sphere. As a first step, the behavior of an elliptic inclusion with an external magnetic field nonparallel to the major axis is to be analyzed and explained, see also Siboni and Ponte Castañeda (2012); Galipeau and Ponte Castañeda (2013a). Figure 4 illustrates the considered problem schematically. The quadratic computing domain has an edge length of 2 with an embedded ellipse having a major axis of 1 and a minor axis of 0.4 length. In accordance to the previous example of Section 4.1 the parameters $E^- = 210$, $\nu^- = 0.3$, $M_s^- = 868$ and $\delta^- = 0.883$ or $\chi_B^- = 767$ characterize the material of the inclusion. $E^+ = 1$, $\nu^+ = 0.4$ and $\chi_B^+ = 0$ are assigned to the nonmagnetizable matrix.
Again, the displacement is set to zero and a linear vector potential with a difference of $\Delta\hat{A}_3 = 2,5$ is prescribed on the whole boundary. Because the magnetic load is not in parallel with the effective field inside the inclusion, a resultant torque is present and tends to align the ellipse with the external magnetic field. This torque, which is equilibrated by the surrounding matrix material, results in a clockwise rotation of the inclusion. The evaluation of the deformation is presented in Figure 6 (a) by means of the angle φ, which is defined in Figure 4. In contrast to the first example, the small deformation model predicts larger rotations, for both the magnetic nonlinear and linear case. This is caused by the proportionality of the torque to the angle between the external magnetic field and the major axis, which decreases with increasing φ. In the small deformation model all calculations are performed with respect to the undeformed reference configuration and thus the net torque is higher. However, the magnetic linear behavior is linked to a high overestimation of the deformation due to the lack of saturation. Figure 6 (b) shows the dependence of the magnetic induction B_1 at the point $X_1 = X_2 = 0$ on the incremental load. The magnetization into the X_1-direction inside the inclusion rises with the alignment and reaches its configuration dependent maximum at an angle of $\varphi = 45$, theoretically. But since the torque becomes smaller and the elastic restoring torsional moment larger with an increasing φ, this state is not achievable.
Altogether the magneto-mechanical coupling effects of the reorientation problem are higher compared to the attraction example. Hence, to limit the deformations the elastic matrix modulus is more than ten times stiffer than the one used in Section 4.1.

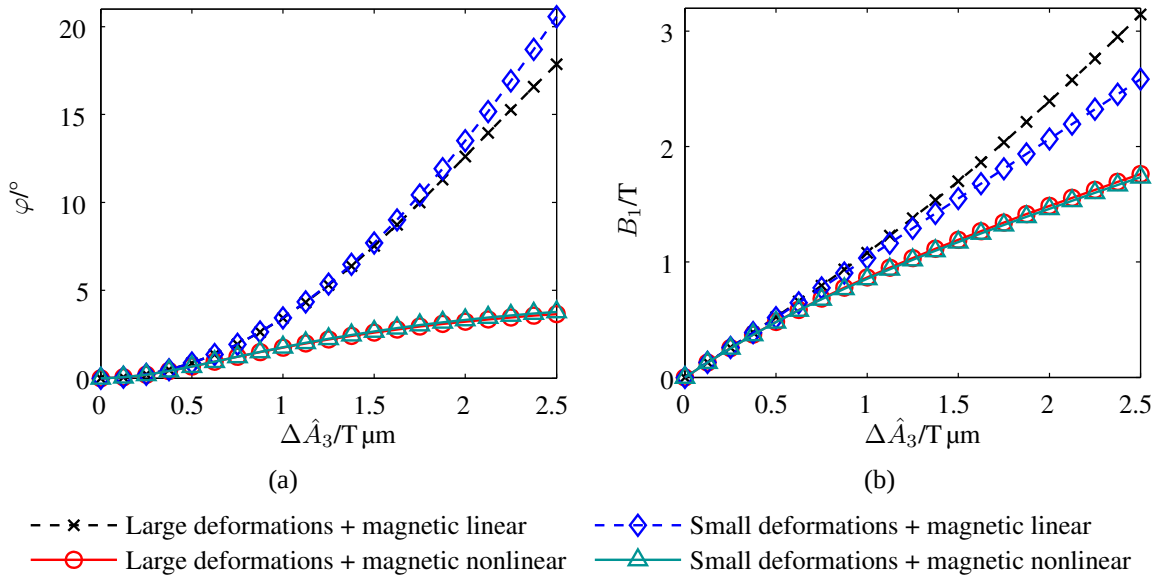

Figure 6. Numerical results for reorientation of an elliptic inclusion: (a) rotation angle of major axis and (b) magnetic induction B_1 at the point $X_1 = X_2 = 0$

5 Conclusion

The main outcome of the present contribution is the constitutive model presented in Section 2.4. It combines the features of finite deformations and large magnetic fields which require a geometric and material nonlinear modeling of MRE at their microscale. Although the considered matrix material is nonmagnetizable and the strains to be expected in the particles are small, a common model facilitates the implementation and enables a further extension, e.g., to a macroscopic material model identified by means of homogenization. Based on magnetization

experiments of carbonyl iron powder, a nonlinear and isotropic phenomenological model is introduced in addition to a linearized approximation. The proposed FE formulation of the nonlinear model for MRE, is an efficient tool for solving coupled magneto-mechanical BVP at the microscopic length scale. Some convergence problems associated with the implemented staggered numerical coupling scheme may be overcome, e.g., by the prediction of incremental changes and numerical relaxation methods as proposed by Erbts and Düster (2012).
The presented results show that there is no significant difference between the small and the large deformation model when using the more sophisticated nonlinear magnetic material (see the corresponding curves in Figures 5 and 6). But in real life situations MRE undergo finite strains mainly induced by mechanical loadings. Under such conditions the internal structure, determined by the arrangement and orientation of particles and clusters of them, changes and must be considered when solving magnetic and coupled mechanical field problems. For small loadings, i.e. values of the magnetic field intensity, the afore shown results coincide. This is a minimum requirement on the extension of our previous work to large deformations. Thus the linear magnetic material behavior seems to be sufficient under such loading conditions.
Current and ongoing work is related to the implementation of the model within an extended FE formulation. It is to be used for solving local BVP of representative volume elements in a homogenization framework in the context of large deformations.

Acknowledgements

This project (ECEMP-B4; SAB: 13854/2379) is funded by the European Union and the Free State of Saxony. We also want to thank Adam, F., Borin, D., Odenbach, S. from TU Dresden, Institute of Fluid Mechanics, for the experimental characterization of the magnetization behavior (Figure 1) and Brummund, J. from TU Dresden, Institute of Solid Mechanics, for providing his in-depth manuscript concerning equations of jump (Brummund (2013)).

References

Belytschko, T.; Liu, W. K.; Moran, B.: *Nonlinear Finite Elements for Continua and Structures*. John Wiley & Sons, Chichester (2000).

Brummund, J.: Eine Notiz zur Ableitung von Sprungbedingungen und Feldgleichungen in einer Fläche aus den zughörigen Feldgleichungen im Raum mittels Distributionen und Anwendungen. To be published (2013).

Bustamante, R.: *Mathematical modelling of non-linear magneto- and electro-active rubber-like materials*. Ph.D. thesis, University of Glasgow (2007).

Bustamante, R.; Dorfmann, A.; Ogden, R. W.: On variational formulations in nonlinear magnetoelastostatics. *Mathematics and Mechanics of Solids*, 13, 8, (2008), 725–745.

Carlson, J. D.; Jolly, M. R.: MR fluid, foam and elastomer devices. *Mechatronics*, 10, 4–5, (2000), 555–569.

Coleman, B. D.; Noll, W.: The thermodynamics of elastic materials with heat conduction and viscosity. *Archive for Rational Mechanics and Analysis*, 13, 1, (1963), 167–178.

Davis, L. C.: Model of magnetorheological elastomers. *Journal of Applied Physics*, 85, 6, (1999), 3348–3351.

de Groot, S. R.; Suttorp, L. G.: *Foundations of Electrodynamics*. North-Holland, Amsterdam (1972).

Dorfmann, A.; Ogden, R. W.: Magnetoelastic modelling of elastomers. *European Journal of Mechanics A/Solids*, 22, 4, (2003), 497–507.

Dorfmann, A.; Ogden, R. W.: Nonlinear magnetoelastic deformations. *Quarterly Journal of Mechanics and Applied Mathematics*, 57, 4, (2004), 599–622.

Erbts, P.; Düster, A.: Accelerated staggered coupling schemes for problems of thermoelasticity at finite strains. *Computers & Mathematics with Applications*, 64, 8, (2012), 2408–2430.

Eringen, A. C.; Maugin, G. A.: *Electrodynamics of Continua I*. Springer, New York (1990).

Galipeau, E.; Ponte Castañeda, P.: A finite-strain constitutive model for magnetorheological elastomers: Magnetic torques and fiber rotations. *Journal of the Mechanics and Physics of Solids*, 61, 4, (2013a), 1065–1090.

Galipeau, E.; Ponte Castañeda, P.: Giant field-induced strains in magnetoactive elastomer composites. *Proceedings of the Royal Society A: Mathematical, Physical and Engineering Science*, 469, 2158, (2013b), 20130385.

Hughes, T. J. R.; Pister, K. S.: Consistent linearization in mechanics of solids and structures. *Computers & Structures*, 8, 3–4, (1978), 391–397.

Jackson, J. D.: *Klassische Elektrodynamik*. Walter de Gruyter, Berlin, 4th edn. (2006).

Kästner, M.; Müller, S.; Goldmann, J.; Spieler, C.; Brummund, J.; Ulbricht, V.: Higher-order extended FEM for weak discontinuities – level set representation, quadrature and application to magneto-mechanical problems. *International Journal for Numerical Methods in Engineering*, 93, 13, (2013), 1403–1424.

Ogden, R. W.: *Non-Linear Elastic Deformations*. Dover, corrected republication, Mineola (1997).

Ponte Castañeda, P.; Galipeau, E.: Homogenization-based constitutive models for magnetorheological elastomers at finite strain. *Journal of the Mechanics and Physics of Solids*, 59, 2, (2011), 194–215.

Rudykh, S.; Bertoldi, K.: Stability of anisotropic magnetorheological elastomers in finite deformations: A micromechanical approach. *Journal of the Mechanics and Physics of Solids*, 61, 4, (2013), 949–967.

Siboni, M. H.; Ponte Castañeda, P.: A magnetically anisotropic, ellipsoidal inclusion subjected to a non-aligned magnetic field in an elastic medium. *Comptes Rendus Mecanique*, 340, 4–5, (2012), 205–218.

Spieler, C.; Kästner, M.; Goldmann, J.; Brummund, J.; Ulbricht, V.: XFEM modeling and homogenization of magnetoactive composites. *Acta Mechanica*, , (2013), Doi: 10.1007/s00707–013–0948–5.

Wriggers, P.: *Nonlinear Finite Element Methods*. Springer, Berlin (2008).

Zienkiewicz, O. C.; Taylor, R. L.: *The Finite Element Method for Solid and Structural Mechanics*. Elsevier, Amsterdam, 6th edn. (2005).

Address: Dipl.-Ing. Christian Spieler, Philipp Metsch, Dr.-Ing. Markus Kästner and Prof. Dr.-Ing. habil. Volker Ulbricht, Institute of Solid Mechanics, Technische Universität Dresden, 01062 Dresden, Germany.
email: Christian.Spieler@tu-dresden.de; metsch@mfk.mw.tu-dresden.de; Markus.Kaestner@tu-dresden.de;Volker.Ulbricht@tu-dresden.de